Proceedings of ASME Turbo Expo 2019: Turbomachinery Technical Conference and Exposition
GT2019
June 17-21, 2019, Phoenix, Arizona

GT2019-90877

PERFORMANCE OF PUBLIC FILM COOLING GEOMETRIES PRODUCED THROUGH ADDITIVE MANUFACTURING

Jacob C. Snyder and Karen A. Thole
Department of Mechanical Engineering
The Pennsylvania State University
University Park, PA, USA

ABSTRACT

Film cooling is an essential cooling technology to allow modern gas turbines to operate at high temperatures. For years, researchers in this community have worked to improve the effectiveness of film cooling configurations by maximizing the coolant coverage and minimizing the heat flux from the hot gas into the part. Working towards this goal has generated many promising film cooling concepts with unique shapes and configurations. However, until recently, many of these designs were challenging to manufacture in actual turbine hardware due to limitations with legacy manufacturing methods. Now, with the advances in additive manufacturing, it is possible to create turbine parts using high temperature nickel alloys that feature detailed and unique geometry features. Armed with this new manufacturing power, this study aims to build and test the promising designs from the public literature that were previously difficult or impossible to implement.

In this study, different cooling hole designs were manufactured in test coupons using a laser powder bed fusion process. Each nickel alloy coupon featured a single row of engine scale cooling holes, fed by a micro-channel. To evaluate performance, the overall cooling effectiveness of each coupon was measured using a matched Biot test at engine relevant conditions. The results showed that certain hole shapes are better suited for additive manufacturing than others, and that the manufacturing process can cause significant deviations from the performance reported in literature.

INTRODUCTION

Metal-based additive manufacturing (AM) has begun to see many uses in the gas turbine industry, from rapid prototyping to production components. The quick speed and design freedom afforded by AM are valuable across the entire engine, although the benefits of additive manufacturing are especially appealing for use in the hot section. Gains in cooling performance have a direct impact to the efficiency of the engine, and therefore is the subject of much development. Turbine designers are constantly working to evolve the state of the art to increase performance of cooling technologies.

One key technology to help limit the heat loads to hot section components is film cooling. As a result of its ubiquity, numerous studies in literature have focused on understanding the physics associated with different film cooling geometries and configurations. Some studies have proposed innovative geometries to improve cooling effectiveness, but their implementation was limited by the manufacturing technology of the time. Now, with the maturation of AM, these concepts can be made out of high temperature nickel alloys at engine scale.

However, one well known consequence of the AM process is high surface roughness. Surface finishing techniques are available to smooth exterior surfaces; however, smoothing internal surfaces can be challenging depending on the geometry and scale of the features. Surface treatment also adds an additional step in the manufacturing process. Moreover, the authors' previous work showed that the as-built surface roughness is beneficial to heat transfer performance in internal cooling [1]. Therefore, it may be desirable to use AM parts with cooling features that are in their as-built state.

In a previous study, the authors investigated the effects of scale and build orientation on the cooling effectiveness of a baseline shaped film cooling hole produced with additive manufacturing [2]. In-hole roughness was shown to have a significant effect on the cooling performance of the hole, increasing the convective benefit but reducing the film benefit. Additionally, the as-built design deviated significantly from the CAD model. These effects could prove to be detrimental when attempting to manufacture novel cooling hole design concepts.

When utilizing AM to create novel cooling holes, two natural questions arise. First, is the performance of the AM hole consistent with the performance of the ideal hole shape developed in the basic laboratory experiments or simulations? Second, which hole features work best when used in an AM implementation?

This study seeks to investigate these questions by manufacturing and testing six different cooling hole designs previously given in the literature. Five novel hole designs and one baseline shaped hole design were manufactured in an engine-scale test coupon to evaluate overall cooling effectiveness. Trends of effectiveness are examined amongst the holes. Additionally, the success of certain geometric features are examined and recommendations made for the design of cooling holes intended for AM.

NOMENCLATURE

A_{AA}	endwall surface area use for averaging
A_c	cross-sectional flow area
Bi	Biot number, $h_\infty t_{wall}/k$
D	film hole metering section diameter
DR	density ratio, ρ_c/ρ_∞
FP	flow parameter, $\dot{m}\sqrt{RT_c}/(P_cA_c)$
h	convective heat transfer coefficient
I	momentum flux ratio, $(\rho_c v_f^2)/(\rho_\infty U_\infty^2)$
k	thermal conductivity
L	hole length
$\dot{m}$	mass flow rate
M	blowing ratio, $(\rho_c v_f)/(\rho_\infty U_\infty)$
Ma	Mach number
Nu	Nusselt number, hD_h/k_{air}
P	spanwise hole spacing
PR	pressure ratio
R	specific gas constant
Re	Reynolds number, vD_h/ν
T	temperature
t	cooling hole breakout width
t_{wall}	coupon wall thickness
U	maximum/centerline velocity
v	flow velocity
X	streamwise distance

Greek

ϕ	overall effectiveness $(T_\infty-T_s)/(T_\infty-T_c)$
$\bar{\phi}$	laterally averaged overall effectiveness
$\bar{\bar{\phi}}$	area averaged overall effectiveness
$\bar{\bar{\phi}}_h$	hole region area average overall effectiveness
ρ	fluid density
ν	kinematic viscosity

Subscripts

avg	averaged
c	coolant condition
design	CAD specified dimension
f	film cooling flow
i	internal microchannel condition
meas	measured from CT scan data
w	external wall condition
∞	mainstream flow condition

REVIEW OF LITERATURE

Few cooling technologies have had as large of an impact on the performance of gas turbine engines as did the introduction of shaped film cooling holes [3]. The use of round holes for film cooling is becoming less common as advances in manufacturing have driven the benefits of a shaped hole to outweigh the increased cost of producing such holes. Because of the impact shaping the exit has on film cooling performance, numerous studies have focused on identifying hole geometries that produce the highest cooling effectiveness.

Goldstein et al. [4] was the first to present a thorough set of quantitative heat transfer measurements of shaped film cooling holes. It was this paper that first showed the ability of shaped cooling holes to resist liftoff and perform better than cylindrical holes. Since then, a vast number of studies have looked at the physics of shaped hole geometries and configurations. Of these numerous studies, a few stand out by proposing novel film cooling hole shapes that push the limits of manufacturing. Since AM affords the design flexibility to create unique designs, these types of studies are of interest for the current study. The literature summary below is by no means an exhaustive list of novel hole shapes. Rather, the studies chosen for this investigation represent different classes of geometric features that may be of interest when designing a new hole specifically to be produced with AM.

Sargison et al. [5] first proposed the design concept of a converging slot film cooling hole (i.e. console). The hole transitions from a cylindrical metering section to a rectangular slot at the exit. Multiple console holes placed with tight spacing allows the exits of adjacent holes to blend into one continuous slot. The intent was to create a slot geometry with discrete feeds to reduce the stress concentrations associated with continuous cooling slots while retaining the aerodynamic benefits of slot cooling. Results showed comparable effectiveness to a fan shaped hole, but with lower aerodynamic losses attributed to the acceleration of the coolant from the converging slot.

Lu et al. [6] measured film effectiveness of a hole shape that transitioned from a round cross section at the inlet to a crescent shaped cross section at the exit. The authors stated that the intent of this hole shape was to reduce the likelihood of main gas path ingestion. The crescent hole was shown to outperform cylindrical holes as well as console holes for all blowing ratios tested.

Both Hossain et al. [7] and Thurman et al. [8] studied the application of fluidic oscillators to film cooling. The concept utilized a wall-attachment fluidic oscillator to achieve a wide lateral spread of coolant from a relatively small cooling hole [9]. Hossain et al. measured both adiabatic effectiveness and heat transfer coefficients to characterize the hole's performance. The fluidic oscillator did achieve the goal of spreading coolant laterally, but negatively augmented the heat transfer coefficient resulting in an overall diminished performance.

The Thurman study [8] investigated another novel cooling hole shape containing spiraled grooves. Similar to the rifling in a gun barrel, the grooves were added to a cylindrical hole to impart a rotation to the coolant exiting the hole. This rotating flow was intended to disrupt the counter rotating vortex pair (CRVP). Results showed the coolant jets from the spiral holes staying better attached to the surface than a cylindrical hole. Additionally, the configuration where the spiral direction alternated between adjacent holes showed stronger cooling than holes with the same spiral direction.

Similar to the spiral hole, disrupting the CRVP was also the goal for the anti-vortex (or tripod) hole proposed by Heidmann and Ekkad [10]. The original design includes a large central cylindrical hole flanked by two smaller cylindrical holes. This design was intended to be easier to manufacture than state of the art shaped holes, but with improved performance over singular cylindrical holes. However, as the hole was developed through a number of different studies [11–14], the configuration shown to perform the best was a tripod configuration of three equally-sized shaped holes. This configuration was shown to outperform a typical shaped hole while using approximately 50% less coolant.

Lastly, as the community tested different shaped holes, and repeatedly showed their improved performance over cylindrical holes, it became clear that a new baseline hole was needed. To fill this need, Schroeder and Thole [15] developed the 777 hole, which has a laidback fan shape. The 777 name refers to the forward and lateral expansion angles of 7°. This hole shape was extensively characterized by the inventors with both heat transfer and flow field measurements to allow detailed comparisons to

other holes. Additionally, the 777 hole was the subject of the authors' previous study investigating AM cooling holes [2].

The current study seeks to add to the literature information on the performance of the aforementioned hole shapes when produced with AM. Specifically, the features proposed amongst the different holes shapes are evaluated for their efficacy in an AM implementation. Therefore, the current study is unique in that it investigates novel film cooling shapes under engine relevant manufacturing and testing conditions.

DESCRIPTION OF TEST GEOMETRIES

Six different cooling hole geometries were studied in this work as previously described in the literature review. The six cooling holes consisted of a baseline shaped hole, 777 [15], and five novel hole shapes including: console [5], crescent [6], oscillator [7,8], spiral [8], and tripod [14]. CAD models of each hole were constructed using geometric information provided in the literature and from the authors to ensure the hole geometries were exactly matched to the original studies. Figure 1 shows images of the CAD model constructed for each of the holes.

The 777 hole, shown in Figure 1a is a baseline shaped cooling hole developed by Schroeder and Thole [15], which has been characterized extensively in the open literature. This hole features a cylindrical metering section, followed by a diffuser with forward and lateral expansion angles of 7°. The inclination angle of the hole is 30°. These geometric parameters were chosen for this hole to be representative of typical shaped cooling holes used in industry.

The console hole, shown in Figure 1b, is defined by a circular inlet which converges to a rectangular slot exit. Since the hole converges, the metering section is located at the exit of the hole. This hole is inclined at an angle of 35°. While the console design is a singular hole, the original study proposed spacing the console holes such that the exits of adjacent holes connect, forming one large slot on the surface.

The crescent hole, shown in Figure 1c, is defined by a cylindrical metering section lofted to a crescent shaped exit. The exit cross-section is larger than the inlet, resulting in an area ratio of 2.1. The entire hole is inclined at an angle of 35°.

The fluidic oscillator hole, shown in Figure 1d, is based off of a wall-attachment type fluidic oscillator [9]. The geometry is comprised of three main sections: a converging entry section, an oscillating section with a main channel and two feedback channels, and an expanding fan shaped exit section. The meter is located between the oscillator section and expanding exit. The fan shaped exit has a lateral expansion angle of 35°. One small change was made to the inlet of the hole to account for the difference in coolant supply configuration between the current study (co-flow supply) and the original study (plenum) [7].

The spiral hole, shown in Figure 1e, can be described as a cylindrical hole with deep rifling. A helical groove with a depth equal to 0.4D is cut at a pitch of 4D per revolution. The inclination angle of the hole is 30°. The original study by Thurman et al. [8] investigated two different configurations: spiral in the same direction and spiral in alternating directions. While the alternating direction configuration was shown to perform best, periodicity could not be achieved with the geometry of the test coupons in the current study. Therefore, the spiral same direction configuration was used in the current study.

The tripod (anti-vortex hole), shown in Figure 1f, features a cylindrical metering section which splits into three separate shaped exits. Each hole is inclined 30° from the surface, with the side holes of the tripod oriented at a 15° compound angle from the center hole. The shaped exits of the hole have a forward expansion of 5° but no lateral expansion. Additionally, the tripod hole investigated in this study includes the manufacturing features as described in Ramesh et al. [14] – small fillets on the entrance to the hole and webbing between the holes.

To emulate gas turbine hardware, the different film cooling hole geometries were printed into test coupons identical to those utilized in previous studies by the current authors [2,16]. These coupons featured a single row of five cooling holes fed by a co-flow cooling channel. The cooling channel dimensions were held constant for each of the hole geometries.

The overall size of the cooling holes was adjusted such that the relevant non-dimensional lengths and spacings were matched to the original studies. Matching the non-dimensional parameters was crucial to allow fair comparisons of effectiveness trends to the original studies. However, the consequence of this choice was differences in the absolute size of the cooling holes, as well as the coupon wall thickness. While differing wall thicknesses will affect the conduction through the endwall into the microchannel, a 1-D thermal analysis showed that the conduction resistance is much smaller than the internal convective resistance. Since the conductive resistance only represents a maximum of 5% of the total thermal resistance, the moderate differences in wall thickness have little impact on the overall cooling results.

Table 1 highlights both the dimensional and non-dimensional differences among the holes. The crescent hole has the largest metering area, while the oscillator has the smallest. On the other hand, the crescent hole was the shortest while the oscillator was the longest. Additionally, the area ratios shown in

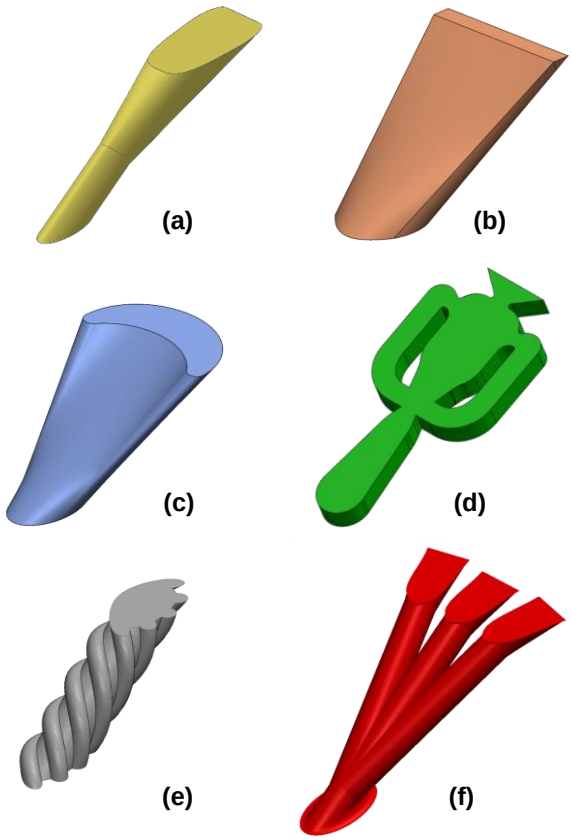

Figure 1. CAD Surfaces of the (a) 777, (b) console, (c) crescent, (d) oscillator, (e) spiral, and (f) tripod film cooling hole geometries.

Table 1 illustrates the different classes of holes. Some holes have constant cross-sections, others expand, while the console hole contracts. These geometric differences are important to understand the results presented in the following sections.

Table 1. Geometric Parameters for the Six Cooling Hole Designs

	P/D	L/D	t/P	D_{meter} (mm)	t_{wall} (mm)	AR	A_{meter} (mm^2)
777	6.0	6.0	0.43	0.76	2.29	2.5	0.46
Console	5.5	7.6	1.0	0.56	3.05	0.51	0.96
Crescent	3.0	3.8	0.89	1.05	2.29	2.1	1.03
Oscillator	8.5	12.0	0.46	0.43	3.05	1.0	0.18
Spiral	6.0	4.0	0.23	0.76	1.52	1.0	0.66
Tripod	6.0	8.0	0.90	0.76	3.05	1.9	0.72

Effect of Additive Manufacturing Process on Geometry

The test coupons were manufactured using Hastelloy-X powder on a common laser powder bed fusion machine. The coupons were oriented such the axis of the cooling hole was aligned with the build direction. Parameters used for the build were adjusted from those used in some of the authors' previous work [2,16] to achieve a better geometric accuracy and lower surface roughness. Details of these parameter changes and effects on cooling can be found in Snyder and Thole [17] .

Despite these improved parameters, it was nonetheless important to characterize the as-built geometry of the coupons. X-ray computed tomography (CT) was used to nondestructively evaluate the internal surfaces of the cooling holes. Each CT scan was performed with a resolution of 45µm, while a software algorithm determined the surface location to within 4.5µm [18].

Figure 2 shows 2D slices taken from the CT scans, bisecting each hole along its mid-plane. White regions indicate solid material, while the red lines indicated the design-prescribed CAD outline for each geometry. Comparing the CAD outlines to the as-built surfaces in Figure 2a-f shows that all of the holes built very close the to the design intent. The largest deviation from the CAD model can be seen in Figure 2d, on the downward facing surfaces near the entrance and exit of the feedback channels in the oscillator hole. This result is not surprising given that downskin surfaces typically have tolerance and roughness issues in L-PBF parts [1,19].

In addition to qualitative characterization, the CT scans were also used to measure the metering area of the cooling holes. Slices were taken along the axis of the cooling holes and cross sectional area was measured for each slice. The minimum area was determined for each hole and then averaged across all five holes in a given coupon. Variation in minimum area for a given geometry was less than 3% except for the console geometry, where the variation was 7%.

To visualize the deviations in metering area from the CAD model, the measured areas are shown in Figure 3 normalized by their respective design-intent area, as given in Table 1. Interestingly, the holes with smallest metering areas printed much closer to the design intent than the holes with larger metering areas. This result is counterintuitive, as the effect of an absolute manufacturing error should diminish with the scale of the feature. However, one explanation is the surface roughness. As the holes increase in size, the surface roughness within the hole has a smaller impact on the dimensions of the meter. The parameters used to build the parts were tuned to the smaller geometries, meaning they over-compensated for the roughness on the larger geometries. Therefore, the AM process parameters should be tuned for the particular geometry being fabricated.

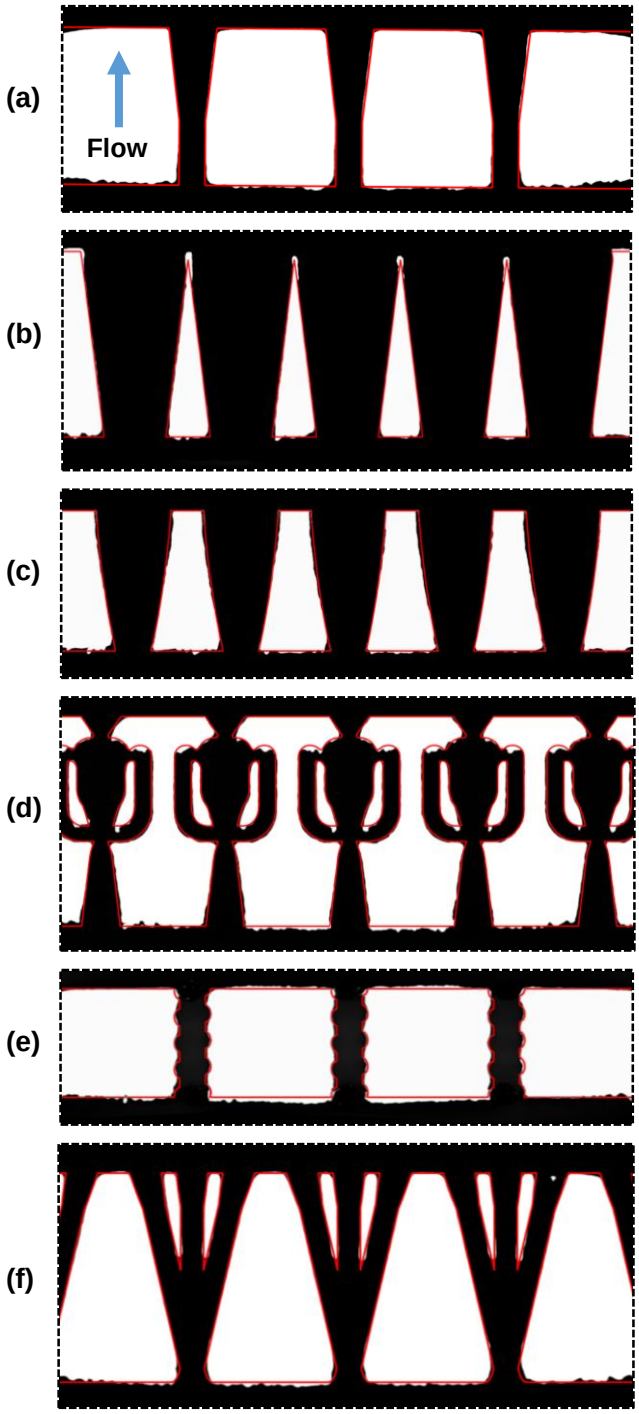

Figure 2. Mid-plane slices of CT scan data comparing as built geometry to CAD model (red) for (a) 777, (b) console, (c) crescent, (d) oscillator, (e) spiral, and (f) tripod holes. Width of slices = 16.75mm. Coolant flow s through the holes from bottom to top of image.

As a final characterization of the coupons, a light microscope was used to examine the exit geometry of the cooling holes. Figure 4 shows images taken of the same surface region of the coupons, with the camera angled to view down the cooling holes' axes.

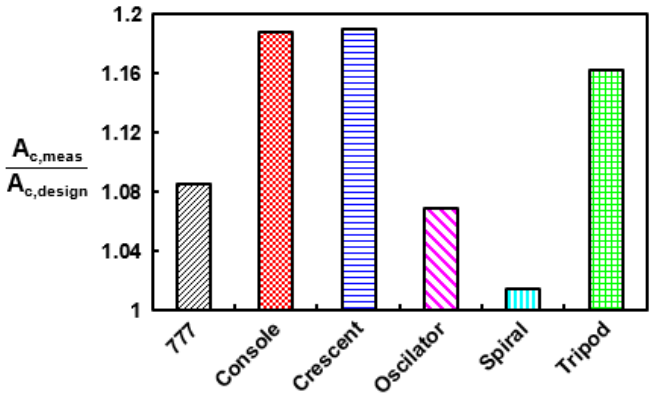

Figure 3. Measured metering area for each hole geometry normalized by the design intent.

The shaped exits of the 777 and tripod holes, Figure 4a and Figure 4f, appear to have been produced cleanly. On the other hand the remaining images in Figure 4 show thin material at the leading edge of the hole deformed to varying extents around the hole exits. For example, Figure 4b shows a slightly smaller slot exit for the holes on the left side of the image. Similarly, the smile shaped exit of the crescent hole, Figure 4c has a slightly different geometry across the five holes. These thin leading edge regions are susceptible to deformation and irregularities in both manufacturing and post-processing. Therefore, improvements to these cooling hole designs should address these thin regions, taking into account the build orientation and manufacturing process.

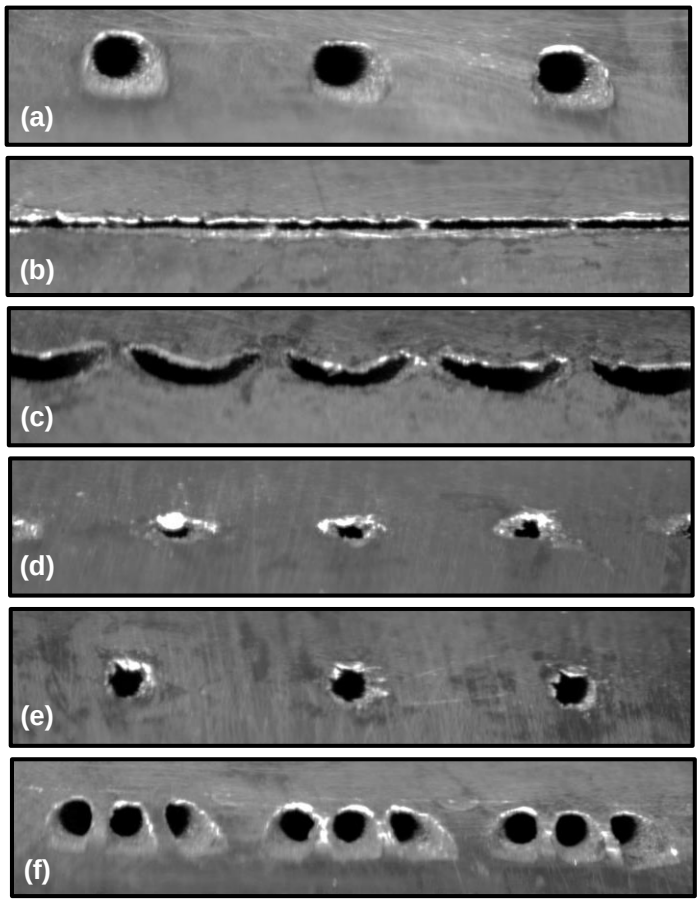

Figure 4. Optical microscope images looking down hole axes of (a) 777, (b) console, (c) crescent, (d) oscillator, (e) spiral, and (f) tripod holes. Width of slices = 15.5mm.

EXPERIMENTAL METHODS

Heat transfer testing on the film cooling coupons was performed in a rig first introduced by Stimpson et al. [2]. A schematic of this rig is shown in Figure 5. A cross-flow of room temperature air was imposed over the surface of the coupon, while coolant was fed to, and exhausted from, the channel within the coupon. Only a portion of the cooling flow exited through the row of cooling holes, imposing a co-flow internal cooling condition, similar to that found in many engine components.

The mainstream flow was supplied by compressed air at a nominal temperature and pressure of 20°C and 4 bar. Alternatively, cooled carbon dioxide (CO_2) gas was used for the coolant in this study to achieve a density ratio, DR = 1.7. The flow rate of the coolant exiting the coupon was measured with a laminar flow element to maintain a constant internal channel Reynolds number, Re_i. For all tests, Re_i was held constant at 14,000 to maintain a similar coolant channel flow condition. The amount of flow exiting through the cooling holes was determined using a flow parameter versus pressure ratio curve generated in a separate experiment, as described in [2].

The non-dimensional parameters Bi and h_∞/h_i were calculated to ensure the applicability of the results to engine components. Both parameters required values of the external (h_∞) and internal (h_i) heat transfer coefficients, which were determined using correlations. The value of h_∞ was estimated using a formulation for developing flow between two parallel flat plates, with one side heated with a constant heat flux obtained from Kays et al. [20]. Details and justification of this formation can be found in the authors' previous study [2]. Values for the internal heat transfer coefficient were estimated from a correlation for convective heat transfer in AM microchannels reported in Stimpson et al. [21]. A full list of non-dimensional parameters defining the experimental conditions is shown in Table 2.

An infrared (IR) camera was used to measure the steady state surface temperature of the coupon. Ten IR images were collected and averaged at each test condition. These images were then converted to a wall temperature using a radiative heat transfer balance, as described in [2].

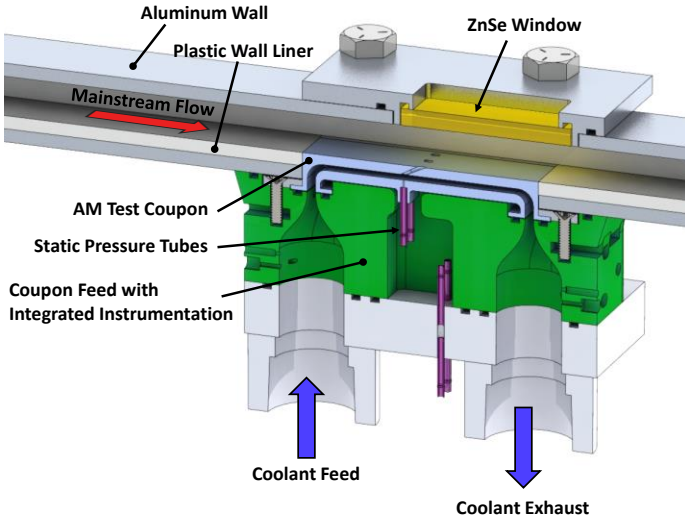

Figure 5. Test rig from Stimpson et al. [2] used for this study.

Table 2. Operating Parameters for Film Cooling Coupons

Parameter	Nominal Value
Bi	0.1
h_∞/h_i	1.0
Ma_∞	0.3
Re_i	14k
M	0.9 – 3.6
I	0.5 – 8.0
DR	1.65

From the IR data, overall cooling effectiveness was calculated using Equation (1), where T_w is the wall temperature measured with the IR camera, T_∞ is the mainstream static temperature, and T_c is the coolant static temperature.

$$\phi = \frac{T_w - T_\infty}{T_c - T_\infty} \quad (1)$$

An uncertainty analysis was performed to determine the accuracy of the film cooling results using the method described by Kline and McClintock [22]. The uncertainty in flow parameter and pressure ratio were 6% and 2% respectively. Using the flow parameter curve to calculate the film mass flow in the heat transfer experiment resulted in an uncertainty of 8% in $\dot{m}_c$. Uncertainty in momentum flux ratio was between 20% for low I and 10% for high I. Lastly, uncertainty in overall effectiveness was calculated to be between $\delta\phi = \pm 0.043$ and $\delta\phi = \pm 0.050$, depending on the temperatures for a given operating condition. Repeatability was established to be within the uncertainty range by duplicating several test conditions for different coupons.

COOLING HOLE FLOW PARAMETERS

Flow performance of the cooling holes is presented in the form of non-dimensional flow parameter versus pressure ratio in Figure 6. As pressure ratio increases, the performance of the holes splits into three distinct groups. The 777, tripod, and crescent holes are grouped together with the highest non-dimensional flow. The oscillator and spiral holes have nearly the same flow at a medium level, while the console hole has the lowest flow of the holes tested. These groupings match with the area ratio of the holes. The diffused holes have the highest flow performance, the contracting hole has the lowest performance, and straight holes are in the middle.

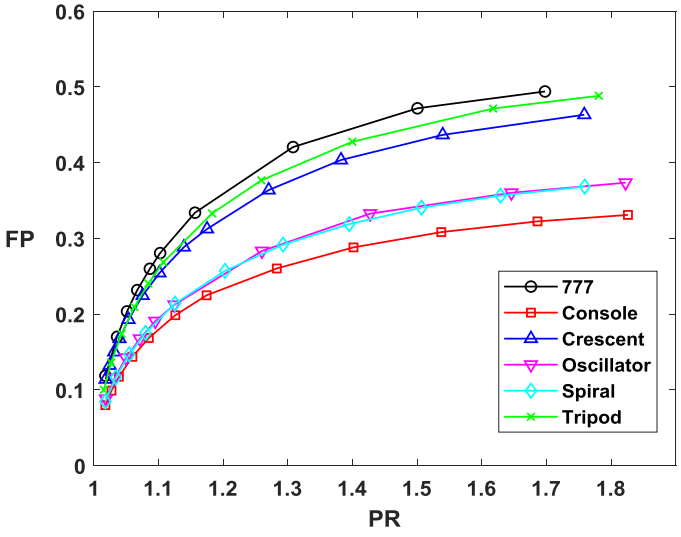

Figure 6. Flow parameter performance for each cooling hole over a range of pressure ratios.

If roughness were playing a role in the flow performance of the cooling holes, it would be expected that the smallest hole (oscillator) would have the largest losses given its highest relative roughness. However, based on the trends shown in Figure 6, it appears that for the roughness magnitudes present in this study, the flow performance is mainly driven by whether the hole expands or contracts.

Ultimately, these flow parameter curves were used to calculate the flow through the film holes during the heat transfer testing based on the pressure ratio applied across the holes.

OVERALL COOLING EFFECTIVENESS COMPARISONS

Overall cooling effectiveness contours at two different momentum fluxes are presented in Figure 7. For each geometry, contours are shown for the three center holes extending a streamwise distance between -5 < X/D < 20. Because of differences in hole spacing and hole size, the physical extent of the non-dimensional regions of interest were different among the different hole geometries, as evidenced in the contour maps in Figure 7. The outer two holes in the row were not considered in any of the analysis herein to eliminate edge effects from the data, but showed similar periodicity to the center three holes.

Immediately evident from the contours in Figure 7 are measurable differences in overall effectiveness among the geometries. Certain holes, such as the console and crescent, show strong effectiveness at both momentum fluxes, while other holes, such as the oscillator and spiral, have relatively weaker cooling. The contours also show that in some cases, such as the 777 and oscillator holes, there are distinct film traces while for the others the jets have merged to provide a more uniform coverage.

Also visible in the data for some of the holes is a non-uniformity in the cooling. In Figure 7b for example, the console hole located around P/D = -5 provides less coolant coverage less than the other two holes in the row. This non-uniformity is due to the slight deviation in the hole exit geometry shown in Figure 4b and is an artifact of the AM process. Given the hole exit is only 0.3 mm, the small deformation of leading edge of the hole had a major impact in the uniformity of the film. Another hole with non-uniform cooling patterns was the crescent hole, as seen in Figure 7c. However, with this hole, only the higher momentum flux case appears to be affected. Considering Figure 4c only shows a slight asymmetry in the exit of the holes, it appears that the effect of small geometric deviations in the crescent shape are exacerbated as the flow through the hole is increased. Therefore, while the console and crescent holes show strong performance, the uniformity of the cooling is highly sensitive to any imperfections that arise from printing small features.

Further examining the effectiveness patterns for the crescent hole shown in Figure 7c, the peaks in effectiveness occur between the holes instead of directly downstream of the holes. This pattern was also seen in the results of Lu et al. [6], although not explicitly addressed in the text. The geometry of this cooling hole, namely the crescent shaped exit, is directing coolant in the spanwise direction. With the holes spaced only 3D apart, the lateral spreading of the coolant accumulates between the holes,

generating a peak in effectiveness. This feature of the crescent hole is highly effective in creating uniform coolant coverage.

The original study by Hossain et al. [7] for the oscillator hole indicated two peaks in adiabatic effectiveness at the corners of the holes from the bi-stable jet. The data for the oscillator hole in the current study, shown in Figure 7d, shows no evidence of these peaks in effectiveness resultant from the oscillation. Whether or not the oscillator was actually sweeping coolant back and forth was difficult to determine from the data collected in this experiment. A separate study by Hossain et al. [23] determined that roughness in the main channel of the oscillator hindered the separation bubble from growing, thereby halting oscillation above a certain flow rate. Their study reported a critical flow rate, which corresponds to the lower end of the range of flowrates used for the testing herein. Given the surface roughness within the AM holes, much of the cooling made possible by the oscillator hole is likely attributed to convection within the hole, as opposed to a sweeping film jet. Specifically, Figure 1d and Figure 2d show how the internal features of the hole extend wider than the exit, providing near surface internal cooling between the holes.

The spiral hole also shows a noticeable change in the cooling patterns between low and high momentum cases in Figure 7e. At the low momentum flux, the film traces are more visible than at high momentum flux, indicating separation of the jets as momentum flux increases. This result agrees with the findings of Thurman et al. [8], where the film effectiveness patterns of the spiral hole indicated jet liftoff at a momentum flux ratio of around two. However, there is a noticeable increase in the convective cooling near the hole at the high momentum condition. The spiral grooves within the hole are acting as ribs, increasing the convection within the hole. This result shows the potential of designing turbulators into AM film cooling holes to enhance the in-hole convection.

The tripod hole, shown in Figure 7f, demonstrates good coolant coverage across the entire span at both low and high momentum conditions. The overall effectiveness levels seen here are quite uniform relative to the adiabatic results of Ramesh et al. [14] indicating the contribution of the convective cooling. Similar to the console and crescent holes, the close spacing of the tripod hole lends to a strong performance. Conventional laser or electro-discharge machining of film-cooling holes are challenged in making tripod holes as a result of the tight tolerances needed for the intersecting holes. The results shown in Figure 7f, however, indicate that AM can successfully construct tripod holes with a favorable performance.

Comparison of Laterally Averaged Effectiveness

For each of the cooling hole geometries, the overall effectiveness data shown in the previous section was averaged across the center hole pitch. Figure 8a and 8b show the laterally averaged data at the low (I=0.5) and high (I=4.0) momentum flux ratios, respectively. In evaluating the lateral averages, it is important to remember that below the surface exposed to the main gas path, there was a co-flowing micro-channel that supplied the coolant to the hole as shown in Figure 5. As such, the sustained high values of overall effectiveness are also a result of the channel cooling below the surface.

For both the low and high momentum flux ratios in Figure 8, the two highest performing cooling holes are the console and the crescent holes while the lowest performing cooling holes were the oscillator, spiral, and 777. The tripod hole falls between the highest and lowest performing holes at both momentum flux

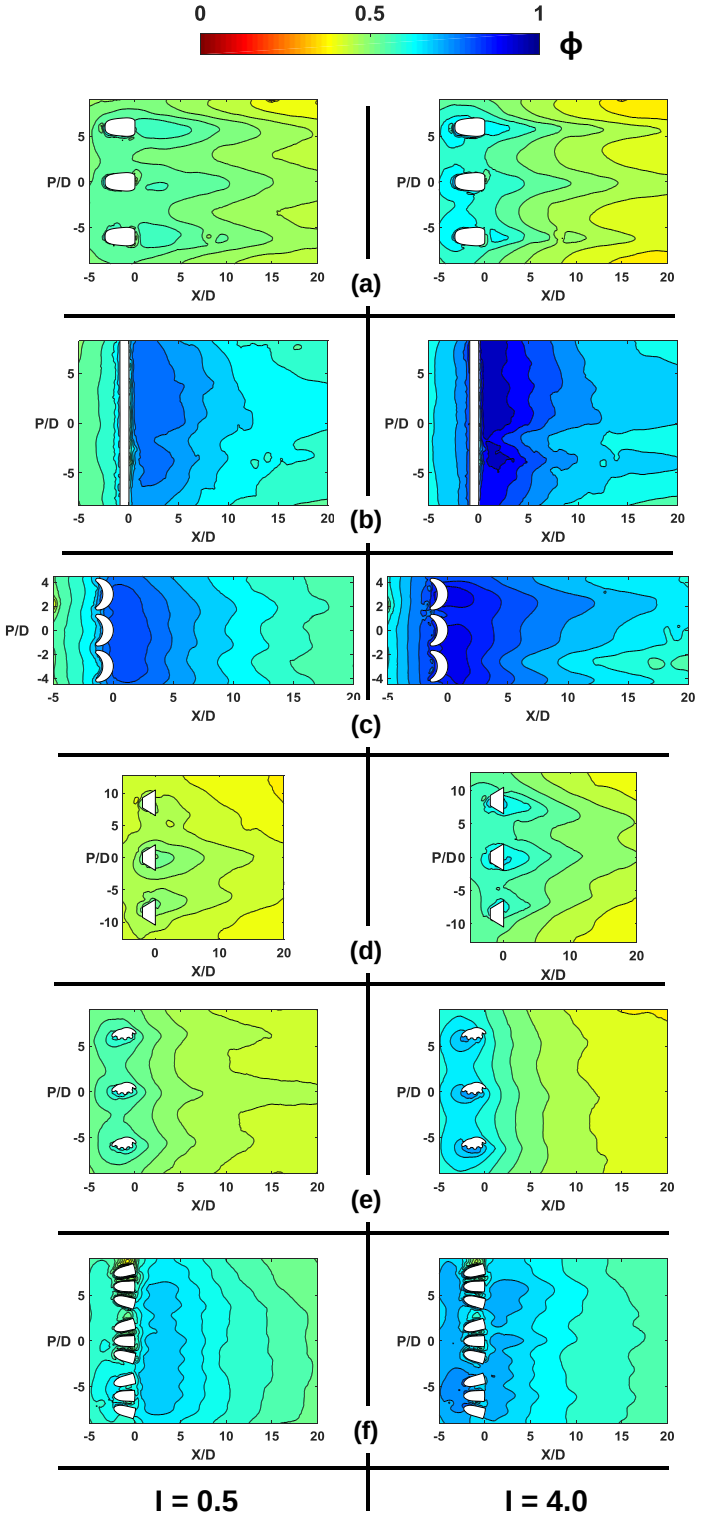

Figure 7. Contours of overall cooling effectiveness at momentum flux ratios of I = 0.5 and 4.0 for (a) 777, (b) Console, (c) Crescent, (d) Oscillator, (e) Spiral, and (f) Tripod holes.

ratios. This result indicates the average coolant coverage for these holes is relatively insensitive to the coolant flow. It is important to note that the 777 hole was not meant to be an optimized hole but rather a basis of comparison for other cooling holes. The 777 represents a modern-day expanded hole, which is a better comparison than a simple round cooling hole due to the jet separation that occurs at high momentum flux ratios.

In Figure 8, the lateral averages of the console and the crescent cooling holes show high values at X/D = 0, which is a result of both the film and convective effects of each hole. At the low momentum flux ratio in Figure 8a, the console and crescent holes have nearly identical performance while at the high momentum flux ratio, the console hole outperforms the crescent hole. For both of these cooling holes, the streamwise decay is also nearly the same until X/D = 12 where the decay for the console hole diverges and is better than the crescent hole. The differences that occur farther downstream can be seen in the contours in Figure 7b and 7c, which can be attributed to the non-uniformity of the coolant flow resulting from the AM defects.

At the low momentum flux ratio in Figure 8a, there is nearly no streamwise decay for the 777 and oscillator holes indicating little contribution of the film. There is a slight decay for the spiral cooling hole, which is interpreted to be an effect of the cooling jet mixing with the mainstream. However, at the high momentum flux ratio shown in Figure 8b, there is a typical film-cooling effectiveness decay with streamwise distance for these holes, with nearly identical performance by both the 777 and oscillator holes.

For the high momentum condition, shown in Figure 8b, the 777 and oscillator holes have nearly identical performance. This is counter to the results of the original study from literature [7], where the oscillator had stronger cooling than the 777 hole, but decayed faster due to the mixing induced by the oscillations. This discrepancy between the current study and the original study trends is attributed to the AM roughness, whereby the oscillator is not working as intended in this implementation.

SCALING OVERALL COOLING EFFECTIVENESS

To determine how the cooling effectiveness scales with operating condition, the coupons were tested over a range of momentum flux ratios. Area averaged effectiveness, $\bar{\bar{\phi}}$, was calculated by averaging data in the region from 0 < X/D < 20 in the streamwise direction, and ± 1.5P in the spanwise direction over the center cooling hole. Figure 9 shows the area averaged effectiveness over the range of momentum flux ratios tested. Note that the large diameters for the crescent and console holes required a significant amount of CO_2 to reach the high momentum conditions resulting in a limit for the maximum momentum flux ratio for these holes, as shown in Figure 9a. As will be discussed in this section, a number of different scaling methods were calculated using the data to compare the performance. Each of these methods provide different figures of merit and can be considered in implementing the cooling hole design. It is also of note to remember that the micro-channel Reynolds number remained constant for all of the conditions, indicating that the convective cooling from the micro-channel can be taken as a constant.

The area-averaged data in Figure 9a compare the different hole geometries across the full range of momentum flux ratios. The data indicate that for all of the holes, cooling performance generally increases with momentum flux ratio. Exceptions are the spiral cooling hole, which decreases in performance slightly before increasing, and the 777 cooling hole, which remains relatively constant with momentum flux ratio. While many cooling holes show a plateau or drop in adiabatic effectiveness at high momentum flux ratios due to jet separation [7,15,24,25], previous studies have shown that the overall effectiveness of AM film holes continues to increase with coolant momentum flux [2,16]. Increased in-hole convection resulting from the AM

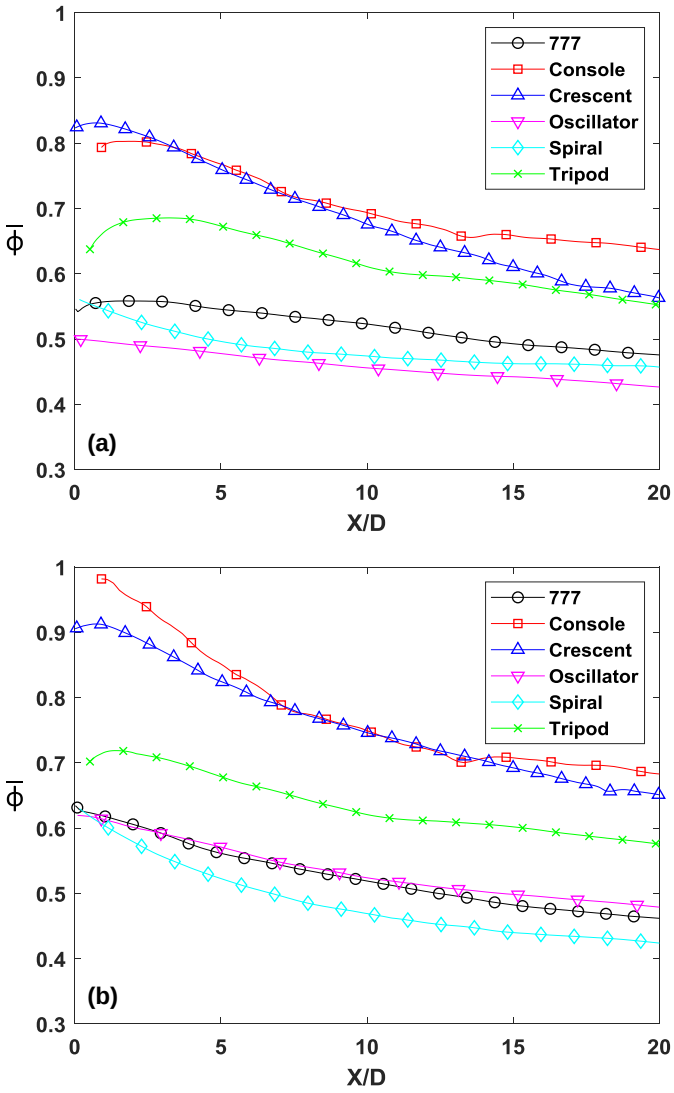

Figure 8. Laterally averaged overall cooling effectiveness for the center hole at (a) I=0.5 and (b) I=4.0.

roughness is hypothesized to offset the decrease in the film effectiveness as the jet lifts-off the surface. As the coolant flow is increased, the in-hole convection effect on cooling increases faster than the film effectiveness decreases. The trends in Figure 9a suggest that the contribution of the in-hole convection across the variety of hole shapes tested in this study is a key benefit of additively manufactured cooling holes and should not be overlooked. In-hole convection effects will be examined in the next section.

Comparing the data within Figure 9a, the different holes separate into three distinct groups: holes with high, medium, and low overall effectiveness. Comparing these groups with the geometric data shown in Table 1, it is clear that the effectiveness scales with the spacing and size of the hole. The smallest, farthest spaced holes perform the worst, while the largest, closely spaced holes perform the best.

One clear factor to take into account is the difference in coolant mass flow used by the holes. At a matched momentum flux ratio, holes with different metering areas will use different amounts of coolant. Additionally, by averaging data over the same non-dimensional region, area averaged effectiveness covers different dimensional surface regions. To account for these

differences, Figure 9b shows the area-averaged cooling effectiveness presented in terms of coolant flow per unit surface area (surface area is also referred to as the external coverage area). The coolant flow per surface area was calculated using the mass flow rate through the middle three holes divided by the area over which effectiveness is being averaged in calculating $\overline{\overline{\phi}}$. Figure 9b is arguably the most useful for a turbine designer, as it indicates how effectively each hole design reduces the surface temperature per unit area for a given flow rate. With this scaling, the crescent shows the best cooling of all of the holes tested, while the spiral shows the worst.

Scaling with coolant flow per surface area in Figure 9b also highlights the difference in the trend of the oscillator compared to the other hole designs. A steep rise in cooling performance occurs relative to the other holes, suggesting a different physical mechanism is driving the cooling. As mentioned previously, it is hypothesized that this design has a stronger in-hole convection due to the geometry of the oscillator.

Despite accounting for the differences between the cooling flowrates, the data shown in Figure 9b is still roughly grouped by hole spacing. To correct for different hole spacing, it is common to consider the coverage ratio (t/P) of the holes. The coverage ratio is defined as the breakout width over the hole spacing, or the percentage of the pitch occupied by the hole. Dividing the area averaged effectiveness by the coverage ratio separates the performance of the individual hole geometry from the performance of a row as a whole. Figure 9c shows the adjusted area averaged effectiveness as a function of the surface mass flux. With a coverage ratio of unity, the console hole drops to become the lowest performing design. On the other hand, the spiral hole shows the highest performance since the hole footprint covers a small percentage of the pitch. Ultimately, Figure 9c shows that the strong area averaged cooling of console and crescent holes can be attributed to the large coverage ratio of these holes.

In-Hole Convection Effects

Since in-hole convection has been hypothesized to be a driver in many of the effectiveness trends addressed earlier, the effectiveness data was analyzed to examine in-hole convection by evaluating the near-hole overall effectiveness measurements. Data from X/D = -5 to the hole exit at X/D = 0 were averaged across the three hole pitches , which is shown in Figure 10 versus coolant mass flow per surface area.

The upstream in-hole convection effectiveness results for four of the six collapse to a common curve in Figure 10. The oscillator hole starts out lower than this group of holes, but rises very quickly with flow rate to join the grouping of other holes. This result corroborates the hypothesis on the trends seen in Figure 9, where the different trends of the oscillator hole were attributed to its difference in internal convection driven by its wide internal surface. On the other hand, the console hole exhibits a noticeably worse performance than the other holes. Since the main difference between the console hole and other designs is its converging cross section, the accelerating flow within the hole is hypothesized to be the cause of the decreased in-hole convection. One explanation for this trend would be the decreased convection at the hole entrance due to the large flow area at this location.

Another explanation of the acceleration effect on heat transfer is the suppression of turbulence within the console hole. The acceleration parameter K was well above the threshold for smooth boundary layer re-laminarization [26], which was the intent of the console hole design. While acceleration of a smooth external boundary layer has been shown to decrease heat transfer [27], the flowfield within the hole is significantly more complex due to its development and the presence of surface roughness. Nonetheless, acceleration has been shown to suppress turbulent

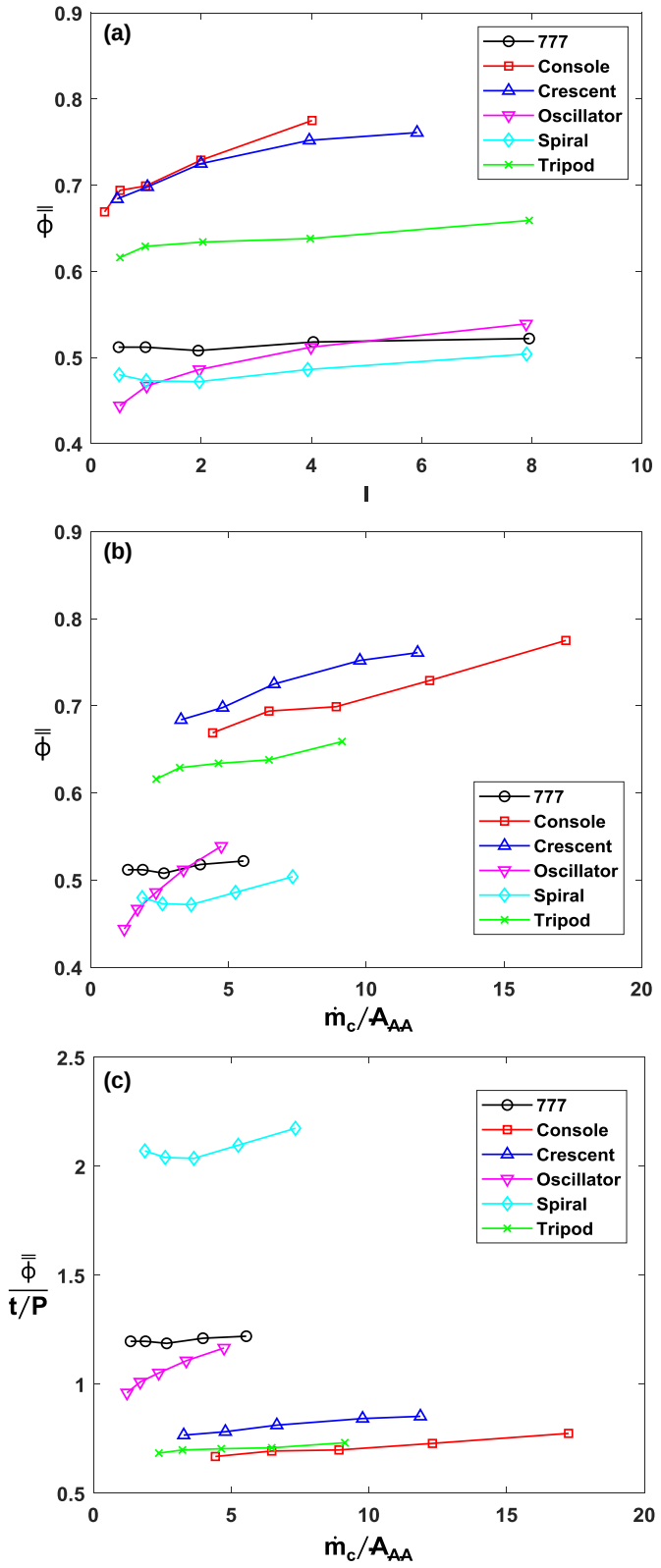

Figure 9. Area averaged overall cooling effectiveness plotted versus momentum flux ratio. The last condition of I=8 was unachievable for the two largest holes, console and crescent, due to limitations with the CO2 coolant supply system.

kinetic energy generation for rough surfaces [28,29], so at a minimum, the console hole is expected to have less turbulent mixing relative to non-converging geometries, ultimately reducing the convective heat transfer within the hole. While the accelerating coolant flow may be desirable from an aerodynamic perspective [30], this benefit must be weighed against the reduction to in-hole convection, as evidenced by Figure 10.

CONCLUSIONS

In this study, six different film cooling hole designs previously presented in the literature were additively manufactured and evaluated for overall cooling effectiveness. Five of the hole designs were novel designs, while the sixth hole design was a baseline shaped cooling hole. Additive manufacturing using Hastelloy-X material was employed to manufacture test coupons containing each of the hole designs at engine scale. The coupons featured a microchannel to feed the film holes in a co-flow configuration.

X-ray computed tomography and optical microscopy allowed characterization of the as-built hole geometry. CT scan results showed most surfaces of the cooling holes printed close to the design intent, owing to the optimal build direction employed. However, microscope images showed deformations of the hole exits for designs featuring thin sections of material, particularly in the case of the console and crescent designs. CT scan measurements indicated the metering areas were oversized for all of the hole designs, with deviations from the CAD metering area as high as 20% for the largest geometries.

Heat transfer testing was performed at conditions to generate a relevant Biot number and internal-to-external convective heat transfer ratio to allow overall cooling effectiveness measurements to be scaled to engine conditions. Results showed that closely spaced holes, such as the console, crescent, and tripod, had the highest coolant coverage. However, the small geometric deviations in the hole exits severely impacted the uniformity of the coolant coverage. When accounting for the differences in scale and coolant mass flow rates between the holes, the crescent hole provided the most cooling per surface mass flux while the spiral hole provided the worst. The results were further scaled by coverage ratio, to determine the hole that provides the best coolant per unit surface area. In this case, the spiral hole had the highest performance, while the console, crescent, and tripod had the lowest performance. These results lead to the conclusion that the success of these three hole designs based on the close hole spacing.

In-hole convection was seen to be a major factor in the performance of the designs, particularly at high coolant flow rates. For example, the roughness inside the oscillator hole prevented the design from performing as an intended oscillating flow, but ultimately provided strong cooling within the hole, offsetting the poor film performance. Considering only the near-hole convective cooling showed comparable performance for all but the console design. The accelerating flow within the hole was hypothesized to reduce the convective heat transfer relative to the other designs.

Overall, this study has demonstrated the ability to manufacture complex cooling hole designs proposed in the literature using additive manufacturing, but also showed that not all cooling holes perform the same as pristine holes tested in laboratories. The results presented herein have identified desirable features to incorporate in additive cooling holes, as well as identified pitfalls to avoid in future designs. For example, the curved cross section of the crescent hole was very effective at spreading the coolant, but the thin upstream section of the design made the hole susceptible to deformations which affected performance. Therefore, turbine designers should consider implementing some of the strong performing design features, while remaining cognizant of the limitations of the AM process in creating the next generation of turbine cooling designs.

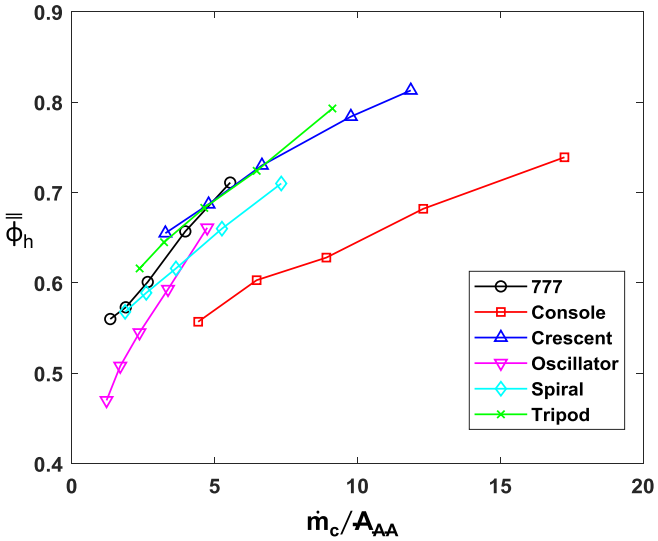

Figure 10. Area averaged overall cooling effectiveness upstream of the hole exit, from -5<X/D <0, versus surface mass flux

ACKNOWLEDGEMENTS

The authors would like to thank Dr. Curtis Stimpson for his assistance in preparing this study, and Mohammad Arif Hossain for providing the CAD model of the oscillator design. The authors also send thanks to Tim Stecko for his assistance with the CT scanning.

The authors would like to thank the U.S. Department of Energy National Energy Technology Laboratory for sponsoring research presented in this paper. This paper is based upon work supported by the Department of Energy under Award Number DE-FE0025011.

REFERENCES

[1] Stimpson, C. K., Snyder, J. C., Thole, K. A., and Mongillo, D., 2016, "Roughness Effects on Flow and Heat Transfer for Additively Manufactured Channels," J. Turbomach., **138**(5).

[2] Stimpson, C. K. C. K., Snyder, J. C., Thole, K. A. K. A., and Mongillo, D., 2018, "Effectiveness Measurements of Additively Manufactured Film Cooling Holes," J. Turbomach., **140**(1), p. 011009.
[3] Bunker, R. S., 2005, "A Review of Shaped Hole Turbine Film-Cooling Technology," J. Heat Transfer, **127**(4), p. 441.
[4] Goldstein, R. J., 1971, "Film Cooling," pp. 321–379.
[5] Sargison, J. E., Guo, S. M., Oldfield, M. L. G., Lock, G. D., and Rawlinson, A. J., 2002, "A Converging Slot-Hole Film-Cooling Geometry—Part 1: Low-Speed Flat-Plate Heat Transfer and Loss," J. Turbomach., **124**(3), p. 453.
[6] Lu, Y., Faucheaux, D., and Ekkad, S. V., 2005, "Film Cooling Measurements for Novel Hole Configurations," *Heat Transfer: Volume 3*, ASME, pp. 59–66.
[7] Hossain, M. A., Prenter, R., Lundgreen, R. K., Ameri, A., Gregory, J. W., and Bons, J. P., 2017, "Experimental and Numerical Investigation of Sweeping Jet Film Cooling," J. Turbomach., **140**(3), p. 031009.
[8] Thurman, D., Poinsatte, P., Ameri, A., Culley, D., Raghu, S., and Shyam, V., 2016, "Investigation of Spiral and Sweeping Holes," J. Turbomach., **138**(9), p. 091007.
[9] Stouffer, R. D., 1979, "Oscillating Spray Device," 4151955A.
[10] Heidmann, J. D., and Ekkad, S., 2008, "A Novel Antivortex Turbine Film-Cooling Hole Concept," J. Turbomach., **130**(3), p. 031020.
[11] Dhungel, A., Lu, Y. P., Phillips, W., Ekkad, S. V., and Heidmann, J., 2009, "Film Cooling From a Row of Holes Supplemented With Antivortex Holes," J. Turbomachinery-Transactions Asme, **131**(2), p. 021007.
[12] Heidmann, J. D., 2008, "A Numerical Study of Anti-Vortex Film Cooling Designs at High Blowing Ratio," Vol. 4 Heat Transf. Parts A B, (November), pp. 789–799.
[13] LeBlanc, C. N., Ramesh, S., Ekkad, S. V., and Alvin, M. A., 2013, "Effect of Hole Exit Shaping on Film Cooling Performance for Tripod Hole Injection Over a Flat Surface," *Volume 3B: Heat Transfer*, ASME, p. V03BT13A011.
[14] Ramesh, S., Ramirez, D. G., Ekkad, S. V., and Alvin, M. A., 2016, "Analysis of Film Cooling Performance of Advanced Tripod Hole Geometries with and without Manufacturing Features," Int. J. Heat Mass Transf., **94**, pp. 9–19.
[15] Schroeder, R. R. P., and Thole, K. A., 2014, "Adiabatic Effectiveness Measurements for a Baseline Shaped Film Cooling Hole," *Proceedings of ASME Turbo Expo 2014: Turbine Technical Conference and Exposition*, ASME, Düsseldorf, Germany, pp. 1–13.
[16] Stimpson, C. K., Snyder, J. C., Thole, K. A., and Mongillo, D., 2018, "Effects of Coolant Feed Direction on Additively Manufactured Film Cooling Holes," J. Turbomach., **140**(11), p. 111001.
[17] Snyder, J. C., and Thole, K. A., 2019, "Effect of Additive Manufacturing Process Parameters on Turbine Cooling," *ASME Turbo Expo 2019: Turbomachinery Technical Conference and Exposition*, Phoenix, AZ.
[18] Becker, B., Maier, D., and Reinhart, C., 2012, "Computer Tomography Has Arrived in Automated Inspection Processes, Combining Material and Geometry Analyses," *Proceedings of The 18th World Conference on Non-Destructive Testing*.
[19] Snyder, J. C., Stimpson, C. K. C. K., Thole, K. a. K. A., and Mongillo, D. J. D. J., 2015, "Build Direction Effects on Microchannel Tolerance and Surface Roughness," J. Mech. Des., **137**(11), p. 111411.
[20] Kays, W., Crawford, M., and Weigand, B., 2004, *Convective Heat & Mass Transfer*, McGraw-Hill, Boston.
[21] Stimpson, C. K., Snyder, J. C., Thole, K. A., and Mongillo, D., 2016, "Scaling Roughness Effects on Pressure Loss and Heat Transfer of Additively Manufactured Channels," J. Turbomach., **139**(2), p. 021003.
[22] Kline, S. J., and McClintock, F. A., 1953, "Describing Uncertainties in Single-Sample Experiments," Mech. Eng., **75**(1), pp. 3–8.
[23] Hossain, M. A., Prenter, R., Agricola, L., Lundgreen, R. K., Ameri, A., Gregory, J. W., and Bons, J. P., 2017, "Effects of Roughness on the Performance of Fluidic Oscillators," 55th AIAA Aerosp. Sci. Meet., (January).
[24] Haydt, S., Lynch, S., and Lewis, S., 2018, "The Effect of Area Ratio Change Via Increased Hole Length for Shaped Film Cooling Holes With Constant Expansion Angles," J. Turbomach., **140**(5), p. 051002.
[25] Saumweber, C., and Schulz, A., 2012, "Effect of Geometry Variations on the Cooling Performance of Fan-Shaped Cooling Holes," J. Turbomach., **134**(6), p. 061008.
[26] Narasimha, R., and Sreenivasan, K. R., 1979, "Relaminarization of Fluid Flows," pp. 221–309.
[27] Moretti, P. M., and Kays, W. M., 1965, "Heat Transfer to a Turbulent Boundary Layer with Varying Free-Stream Velocity and Varying Surface Temperature—an Experimental Study," Int. J. Heat Mass Transf., **8**(9), pp. 1187–1202.
[28] He, S., and Seddighi, M., 2013, "Turbulence in Transient Channel Flow," J. Fluid Mech., **715**, pp. 60–102.
[29] Coleman, H. W., Moffat, R. J., and Kays, W. M., 1981, "Heat Transfer in the Accelerated Fully Rough Turbulent Boundary Layer," J. Heat Transfer, **103**(1), p. 153.
[30] Sargison, J. E., Guo, S. M., Oldfield, M. L. G., Lock, G. D., and Rawlinson, a J., 2001, "Nozzle Guide Vane Heat Transfer and Loss," ASME Turbo Expo, pp. 1–14.